

SLAC-PUB-7238

August 1996

**An estimate of gas resorption in the damping rings of
the Next Linear Collider***

Frank Zimmerman

Stanford Linear Accelerator Center
Stanford University, Stanford, CA 94309, USA

We express the gas resorption in a high-energy electron or positron storage ring in terms of the photoemission and the electron-induced gas-desorption yields of the vacuum-chamber material. The derived expression is used to estimate the gas resorption in the two main damping rings of the Next Linear Collider (NLC) and, in particular, its dependence on the height of the slots which connect the beam pipe proper to an antechamber.

Submitted to Nuclear Instruments and Methods in Physics Research A

*Work supported by Department of Energy contract DE-AC03-76SF00515.

1 Introduction

The operating vacuum pressure of most high-energy electron or positron storage rings is determined by the dynamic gas load due to photodesorption [1, 2, 3]. Photodesorption manifests itself in a characteristic pressure rise which is proportional to the beam current. The average pressure and, hence, also the photodesorption rate are of critical importance to the performance of an electron or positron storage ring: scattering of electrons off the residual gas has limited the beam lifetime and the equilibrium beam emittance in many synchrotron-light sources and electron-positron collider-rings [4], while, at higher pressure, violent beam-ion instabilities are prone to develop [5, 6, 7]. Therefore, the design of a storage-ring vacuum system should be optimized so as to reduce the rate of photodesorption. Although a wealth of experimental measurements and operational experience with photodesorption in accelerators has been accumulated over the years, simple analytical or semi-analytical formulae which could serve as a guideline for optimization are scarce, and in the design of a new ring the gas-desorption coefficient is commonly only considered as an empirical ‘effective engineering value’ [3].

Inspired by a suggestion in Ref. [8], in this article we express the photodesorption coefficient of a storage ring, which we define as the average number of desorbed molecules per emitted synchrotron photon, in terms of two more fundamental quantities: the photoemission yield and the electron-induced gas-desorption yield of the vacuum-chamber material. These two yields represent the average number of electrons emitted per photon and the average number of desorbed molecules per incident electron, respectively. Both are functions of the projectile energy and of the angle of incidence. And both can readily be measured in the laboratory.

As an illustration, in the third section of this report we will use the

derived formula to estimate the photodesorption coefficient for the two main damping rings [9] of the Next Linear Collider (NLC) [10]. In particular, we will determine the dependence of the resorption coefficient on the height of the coupling slots which connect the beam pipe with the antechamber.

2 The Resorption Coefficient

We consider a general storage ring equipped with an antechamber that is designed to absorb a large fraction of the emitted synchrotron radiation. The molecular conductance and pumping speed in this antechamber are assumed to be so large that photons reaching the antechamber, as well as the molecules they desorb, do not contribute to the pressure inside the beam pipe. However, some photons are emitted at a wide enough angle perpendicular to the horizontal plane of motion that they miss the absorber slots connecting the beam pipe to the antechamber. These photons impinge on the vacuum-chamber wall of the beam pipe proper. The smallest emission angle at which this happens is a function of the location, the beam-pipe geometry, and the slot height. It also depends on magnet misalignments and vertical closed-orbit distortions.

When striking the chamber wall, some of the photons generate photoelectrons which in turn, if they are sufficiently energetic, can desorb gas molecules or atoms. It is generally believed and supported by experiments [1, 11,8,2, 12] that the predominant part of gas resorption in a storage ring is due to these photoelectrons. Therefore, in this paper, we only consider gas resorption induced by photoelectrons and we neglect all other sources of gas load, such as direct photodesorption or thermal outgassing, whose contribution is assumed to be insignificant in comparison [2].

We note that for an infinitely high absorber slot this assumption would not be true. In this case, the gas load would solely be due to thermal outgassing, provided that the return flow of desorbed molecules from the antechamber into the beam pipe remained negligible. As a result, the vacuum pressure would not depend on the beam current. To our knowledge, no high-energy electron storage ring has yet been operated in such a regime.

In order to set the stage for the further discussion, we now introduce the desorption coefficient η . Following Sands [13], the number of photons radiated per radian and per electron is given by

$$N_{\gamma,tot} = \frac{5}{2\sqrt{3}} \gamma \alpha \quad (1)$$

where α denotes the fine-structure constant, and $\gamma \equiv E/(m_e c^2)$ the electron energy in units of the rest energy; E is the beam energy, m_e the electron mass and c the velocity of light. We have used the suffix ‘*tot*’ (*total*) to indicate that the quantity $N_{\gamma,tot}$ includes all photons, *i.e.*, photons emitted at an arbitrary angle. By means of Eq. (1), the total photon emission rate of the entire beam can be written as

$$\dot{N}_{\gamma,tot} = 2\pi \frac{5}{2\sqrt{3}} \frac{\alpha \gamma N_e c}{C} = 8.1 \times 10^{20} \frac{E}{\text{GeV}} \frac{I}{\text{A}}. \quad (2)$$

Here, N_e denotes the number of particles in the bunch, I the average current, C the ring circumference, and the tilde over $\dot{N}_{\gamma,tot}$ signifies that this quantity refers to the full beam and not to a single electron. Since the gas load due to photodesorption, Q_{gas} , is proportional to the photon-emission rate, $\dot{N}_{\gamma,tot}$, it is conveniently expressed in the form [3]

$$\begin{aligned} Q_{gas} = \eta \dot{N} &= \eta 8.1 \times 10^{20} \frac{E I}{\text{GeV A}} \left[\frac{\text{molecules}}{\text{s}} \right] \\ &\approx \eta 24.2 \frac{E I}{\text{GeV A}} \left[\frac{\text{Torr l}}{\text{s}} \right] \end{aligned} \quad (3)$$

where E designates the beam energy (in GeV) and I the beam current (in A). To arrive at the far right-hand-side of Eq. (3) we have used the conversion factor 3×10^{20} Torr L / molecule [3], which is valid for an ideal gas. The desorption coefficient η is defined as

$$\eta \equiv \frac{\text{average number of desorbed molecules}}{\text{radiated photon}}. \quad (4)$$

It is this quantity that we want to calculate. The coefficient η depends on a variety of parameters, such as the vacuum-chamber material, material preparation, exposure to radiation, photon angle of incidence, and photon energy. For this reason, it is often considered as an ‘effective engineering value’ [3].

To derive an analytical expression for the resorption coefficient η , we start from the classical angular and energy spectrum of the synchrotron radiation, which is expressed by the well known formula [14, 15, 16]

$$\frac{d^2 N_\gamma}{d\omega d\Omega} = \frac{1}{3\pi^2} \alpha \omega \left(\frac{\rho}{c}\right)^2 \left(\frac{1}{\gamma^2} + \theta^2\right)^2 \left[K_{2/3}^2(\xi) + \frac{\theta^2}{1/\gamma^2 + \theta^2} K_{1/3}^2(\xi) \right] \quad (5)$$

where

$$\xi \equiv \frac{\omega\rho}{3c} \left(\frac{1}{\gamma^2} + \theta^2\right)^{3/2}, \quad (6)$$

and N_γ is the number of photons, ω the angular frequency, and Ω the solid angle; the symbols $K_{2/3}$ and $K_{1/3}$ denote modified Bessel functions. The angle θ is the latitude with respect to the horizontal plane and not the polar angle.

Equations (5) and (6) show that the typical emission angle θ depends on the photon frequency ω . The rms angular spread of photons at frequency ω (assuming $\omega < \omega_c$) is roughly [16]

$$\theta(\omega)_{\text{rms}} \sim \frac{1}{\gamma} \left(\frac{\omega_c}{\omega}\right)^{1/3} \quad (7)$$

where $\omega_c \equiv 1.5 \gamma^3 c / \rho$ denotes the critical frequency, as defined by Sands [13]. According to Eq. (7), low-energetic photons are emitted at much larger angles than high-energetic ones, and, for this reason, it is primarily the low-energetic photons which are not captured in the antechamber and which, thus, can contribute to the vacuum pressure. Averaging Eq. (7) over all photon energies gives the total rms angular spread of the synchrotron radiation: $\langle \theta_{\text{rms}} \rangle_\omega \approx 1/\gamma$.

It is interesting to note that the radiation spectrum of Eq. (5) is no longer valid at very low frequencies when the photon wavelength becomes comparable to the beam-pipe diameter [17]. In a typical application, the frequency at which the two are equal is exceedingly small, $\omega \leq 10^{-9} \omega_c$, however, and, hence, this effect is of no concern for us.

The number of photons emitted per radian at an angle larger than a certain minimum angle θ_{min} is obtained by numerical integration of Eq. (5),

$$N_\gamma(\theta > \theta_{min}) \simeq 2 \int_0^\infty d\omega \int_{\theta_{min}}^{\pi/2} d\theta \frac{d^2 N}{d\omega d\Omega}, \quad (8)$$

where the factor 2 accounts for both upward and downward emitted photons, and we have made the approximation $d\Omega = \cos \theta d\theta \approx d\theta$, since the typical emission angles θ are very small.

Integration over the product of the synchrotron radiation spectrum $d^2 N/d\omega/d\Omega$ and the photoemission yield $\eta_{pe}(\hbar\omega)$ gives the number of photoelectrons generated per electron and radian:

$$N_{pe}(\theta > \theta_{min}) \simeq 2 \int_0^\infty d\omega \int_{\theta_{min}}^{\pi/2} d\theta \frac{d^2 N}{d\omega d\Omega} \eta_{pe}(\hbar\omega). \quad (9)$$

Here \hbar denotes Planck's constant divided by 2π .

Published low-temperature energy spectra of photoelectrons for different photon frequencies [18] show the existence of a fairly well defined threshold energy, below which no photoelectrons are emitted [18]. This threshold is known as the photoelectric workfunction Φ of the material. For somewhat higher frequencies, the energy spectrum of photoelectrons generated by a monoenergetic photon beam has a characteristic width of the order of 1 eV and the frequency of its peak value increases about linearly with the incident photon energy [18]. For our purposes here, it is then a good approximation to assume that the energy of an emitted photoelectron, E_{pe} , is equal to the difference of the photon energy $\hbar\omega$ and the material workfunction Φ : $E_{pe} \approx (\hbar\omega - \Phi)$.

To derive an estimate for the number of molecules desorbed per electron and radian we now multiply the integrand in Eq. (9) with the yield for electron-induced gas resorption at energy E_{pe} , $\eta_{egd}(E_{pe})$,

$$N_{mol}(\theta > \theta_{min}) \simeq 4 \int_0^\infty d\omega \int_{\theta_{min}}^{\pi/2} d\theta \frac{d^2 N}{d\omega d\Omega} \eta_{pe}(\hbar\omega) \eta_{egd}(\hbar\omega - \Phi), \quad (10)$$

where we have introduced an additional factor of 2 to account for the fact that molecules can be desorbed, with equal probability, both during the creation and the absorption of a photoelectron [1].

Finally, to estimate the resorption coefficient η , defined in Eq. (4), we have to average $N_{mol}(\theta > \theta_{min})$ over the different values of θ_{min} around the ring. Since the resorption coefficient is defined as the number of molecules desorbed per emitted photon, and not as the absolute number of desorbed molecules per electron and per radian, we also have to divide by the total number of photons emitted per electron and per radian, $N_{\gamma,tot}$, of Eq. (1). The final expression for the resorption coefficient is

$$\eta = \frac{\int_C ds N_{mol}(\theta > \theta_{min}(s))}{C N_{\gamma,tot}}, \quad (11)$$

where the term N_{mol} was defined in Eq. (10)—with the spectrum $d^2 N/d\omega/d\Omega$ as given in Eq. (5)—, and $N_{\gamma,tot}$ was introduced in Eq. (1). The angle $\theta_{min}(s)$ denotes the location-dependent minimum emission angle for which a photon misses the absorber slot. The variable s is the position around the ring, and C is the ring circumference. Obviously, in order to apply Eq. (11), or Eq. (10), one must know the photoemission yield η_{pe} and the electron-induced resorption yield η_{egd} as functions of photon or electron energy, respectively. Both these quantities are relatively easy to measure in the laboratory. In addition, when evaluating the resorption coefficient, Eq. (11), also the detailed geometry of the beam pipe and absorber slots and their distribution around the ring, realistic magnet misalignments, and estimated closed-orbit

distortions must be taken into account. In the following section, we describe an exemplary application for the NLC damping rings, in which the three Equations (11), (9) and (10) are evaluated by numerical integration, using approximations to the measured photoemission and electron-induced resorption yields.

Before embarking on this discussion, a few more comments on the two functions η_{pe} and η_{egd} may be appropriate. The photoemission yield η_{pe} is a function not only of the photon energy, but also of the material history, the temperature, and, in particular, the angle of photon incidence; for grazing incidence, the photoemission can either be enhanced, by up to a factor of 10 or even 50 [1], or greatly be reduced, due to total reflection at small photon energies [8]. The detailed dependence of η_{pe} on energy and angle of incidence must be measured carefully for the specific vacuum chamber material and geometry of interest, if a precise estimate of the absolute value of gas resorption is desired.

The electron-induced gas resorption yield η_{egd} appears to be at least as uncertain as the photoemission yield η_{pe} . Its value varies by many orders of magnitude depending on prior exposure to gas or synchrotron radiation, bake-out history, temperature, angle of electron incidence, and many other parameters. In addition, the measured gas resorption in a storage ring is known to decrease strongly with the time of operation [19]. In view of all these uncertainties, it appears legitimate to arrive at a first rough estimate for the resorption coefficient η by assuming the photoemission yield for perpendicular incidence. The latter is widely published for most materials and different material treatments.

It is important to realize that the thereby introduced large uncertainty in the *absolute* value of our result does not preclude fairly reliable

estimates for its *relative* dependence on certain parameters. In other words, even though we may not be able to accurately predict the absolute value of the resorption coefficient, we can calculate its dependence on relevant storage-ring and beam-pipe parameters, such as the beam-pipe radius or the height of the absorber slots. This is very interesting for a design optimization, as illustrated in the following application.

3 Resorption in the NLC Damping Rings

In this section, we evaluate the gas resorption coefficient η of Eq. (11) for the proposed NLC Damping Rings [9, 10] and determine its dependence on the height of the coupling-slots to the antechamber.

The NLC main damping rings are part of the design for a next-generation linear electron-positron collider with a variable cms energy between 500 GeV and 1.5 TeV [10]. The two main damping rings (one each for electron and positron beams) are designed to damp incoming trains of 90 bunches to a very small **vertical** emittance of $\gamma\epsilon_y \leq 3 \times 10^{-8}$ m. After extraction from the rings, the bunch trains are accelerated in the NLC main linacs to an energy of 250–750 GeV, before they are collided at the interaction point. The NLC damping rings operate at a beam energy of 2 GeV. In each ring, four bunch trains are stored simultaneously; every 5.6–8.3 μ s one of the four trains is extracted and a new train injected. Some parameters of the main damping rings are listed in Table 1. The optical lattice of the rings is based on detuned Theoretical Minimum Emittance (TME) cells. The standard arc cell has a length l of 3.9 m and consists of 3 quadrupoles and 1 bending magnet. The bending magnet is 68.4 cm long and has a field of 15.3 kGauss; these numbers translate into a bending angle α_B of 157 mrad and a bending radius ρ of 4.4 m. The bending magnet is conceived as a ‘C’ magnet, which allows an antechamber to exit the outer side of the magnet. The cell layout is depicted in Fig. 1.

In the design, the vacuum chamber of the damping rings is made from aluminum. However, the chamber of the positron ring will possibly be coated by some other material on the inside, to counteract a predicted coupled-bunch instability which is caused by photo- and secondary electrons (‘Ohmi effect’) [20, 21]. The damping-ring beam pipe is circular with a radius r of 1.25 cm.

The coupling-slot that connects the beampipe with the antechamber has a half height w of 2.5 mm, which is tapered to 4 mm in the antechamber itself. The primary photon stop is placed at the end of the antechamber. Figure 2 shows a cross section through the arc vacuum chamber inside a quadrupole magnet.

For a resorption coefficient of 2×10^{-6} molecules per photon and a total pumping per cell of 3200 l/s, the average vacuum pressure in the arc beam chamber is expected to be less than 1 nTorr [10]. A pressure of this order is necessary to keep the ion-induced tune shift across the bunch train below 0.01, and also to suppress a predicted fast beam-ion instability [7]. More detailed information on the design of the NLC damping rings and their vacuum system can be found in Refs. [9] and [10].

The antechamber of the NLC Damping Rings is presently designed to absorb 99.8% of the photon energy from synchrotron radiation. However, a significant fraction of the photons, about 7% and primarily low energetic, will be radiated at angles large enough to strike the vacuum chamber.

The minimum emission angle θ_{min} at which a photon impinges on the vacuum chamber depends on the coupling-slot half height w , on the distance between two adjacent bending magnets, and also on the location of the emission. Specifically, depending on the location within the bending magnet it is given by one of the following three expressions:

$$\theta_{min}(\alpha) = \begin{cases} w/\sqrt{2\rho r} & \text{for } \alpha > \arccos\left(\frac{1}{1+r/\rho}\right) \\ w/(\frac{r}{\sin\alpha} + \rho \tan \frac{\alpha}{2}) & \text{for } r/l < \alpha < \arccos\left(\frac{1}{1+r/\rho}\right) \\ w/l & \text{for } \alpha \leq r/l, \end{cases} \quad (12)$$

where α denotes the azimuthal position across the bend (in radian), measured backwards from the bend exit face (see Fig. 3), ρ is the bending radius, l the cell length, and r the beam pipe radius. The three different expressions refer to the three cases that the radiation hits the chamber inside the same

bend, in the downstream straight section or in the following bend. This is illustrated by the schematic in Fig. 3. In Fig. 4 is shown the variation of the minimum emission angle θ_{min} , Eq. (12), across the bend for three different values of the slot half height w .

According to Eq. (1), in the bending magnets of the NLC damping rings, each electron emits an average number $N_{\gamma,tot}$ of 42 photons per radian. The critical frequency ω_c of this radiation is $6 \times 10^{18} \text{ s}^{-1}$ and corresponds to a photon energy of 3.8 keV. The rms vertical emission angle is $\sim 1/\gamma \sim 260 \mu\text{rad}$. In Fig. 5, the number of photons incident on the inside of the vacuum chamber per radian and electron, Eq. (8), is displayed as a function of the minimum emission angle θ_{min} . We note the strong sensitivity to the minimum angle θ_{min} , which, when combined with Fig. 4, suggests that the main contribution to gas resorption comes from the small fraction of photons emitted at the the very end of a bend, which pass through the straight section and reach the next bending magnet, *i.e.*, those emitted at $\alpha \leq 0.003$ rad in Fig. 4.

We approximate the measured photoemission yield η_{pe} of aluminum [1, 22, 23, 12] by the expression

$$\eta_{pe}(E_\gamma) \approx \begin{cases} (E_\gamma - 4 \text{ eV})/(80 \text{ eV}) & \text{for } 4 \text{ eV} < E_\gamma < 20 \text{ eV} \\ 0.2 (E_\gamma/20 \text{ eV})^{-0.59} & \text{for } E_\gamma > 20 \text{ eV} \end{cases} \quad (13)$$

where 4 eV is the work function Φ of aluminum. In this approximation, the photoemission rises from zero at 4 eV to 20% at 20 eV. It then decreases linearly on a log-log scale and reaches 0.2% at 50 keV. Figure 6 compares the parametrization (13) with some exemplary measurements found in the literature.

Using the approximation (13), we can calculate the number of photoelectrons created per electron and per radian by numerical integration of Eq. (9). The result is depicted in Figure 7, which allows us to estimate the aver-

age photoelectron current in the beam pipe. Most of the photoelectrons are generated by those few photons which are emitted over the last 0.003 radians of the bend (case 3 in Fig. 1), because they have a much higher probability to impinge on the beam-pipe chamber, and, more importantly, the average energy of those which do is much higher than for photons emitted further upstream. Assuming a slot half height w of 2.5 mm, the minimum emission angle θ_{min} for the former is $\sim 600 \mu\text{rad}$ (see Fig. 4). From Fig. 7, the corresponding number of photoelectrons per radian and electron is about 0.1. Multiplying this number with the bend region of interest ($\Delta\alpha \sim 0.003$ rad), and with the beam current (1.2 A), and dividing by the cell length (3.9 m), we estimate that the photoelectron current in the NLC damping rings is less than $100 \mu\text{A m}^{-1}$. By contrast, for PETRA with a factor 6 smaller total beam current (180 mA), with a 7 times higher beam energy (14 GeV) and without dedicated radiation absorbers, the photoelectron current was estimated to be 250 mA m^{-1} [1], *i.e.*, it was more than three orders of magnitude higher than in the proposed damping-ring design. This enormous reduction in the photoelectron current (and, thus, also in the gas resorption) is mainly due to the antechamber, since the effects of the different beam energy and the different beam current in the two rings roughly cancel each other.

We now parametrize the measured electron-induced gas-desorption yield η_{egd} of aluminum [24, 25, 8] by

$$\eta_{egd}(E_e) \approx 0.5 \times \begin{cases} E_e/600 \text{ eV} & \text{for } E_e < 600 \text{ eV} \\ 1 & \text{for } E_e > 600 \text{ eV} \end{cases} \quad (14)$$

where E_e is the electron energy. In Fig. 8, this approximation to η_{egd} is compared with two measurements. Again, the published values vary over a wide range, and the used approximation falls roughly in the middle between the measured yield without prior bake-out and that observed after a 24-hr bake-out at 300 °C. With the help of Eq. (14), we can numerically integrate

Eq. (10) to obtain the number of desorbed molecules per electron and per radian as a function of the minimum emission angle, depicted in Fig. 9.

As our final result, Fig. 10 presents the (initial) resorption coefficient η for the NLC main damping rings, computed by numerical integration of Eq. (11), assuming the above parametrizations for η_{pe} and η_{egd} . Earlier in this report, we have argued that, since the coefficient η decreases strongly with the accumulated photon dose, the absolute value of our estimate will be of less interest than its dependence on the slot half height w . Serendipitously, even the absolute value for zero slot height of about 0.01 is not inconsistent with published data for photodesorption without prior exposure [19].

In the present damping-ring design, the slot half height is 2.5 mm. Because of chamber misalignments and orbit distortions of $\pm 500 \mu\text{m}$ and an rms vertical beam size of $400 \mu\text{m}$, the effective slot half height is almost 1 mm smaller than the actual height [26], *i.e.*, the effective half height is only about 1.5 mm, which, according to Fig. 10, translates into an initial resorption coefficient of 10^{-4} . If we blindly extrapolate from the measured dependence of the resorption coefficient on the radiation exposure time in Ref. [19], the resorption coefficient is expected to decrease by a factor of 50 and to reach its design value of $\eta = 2 \times 10^{-6}$ in about one hour of operation at nominal current, or after a photon dose of $3 \times 10^{22} \text{m}^{-1}$. However, since more than 90% of the photons are absorbed in the antechamber and not in the beam pipe, this estimate appears too optimistic, by at least a factor of 10.

Figure 10 suggests that in order to reduce the initial resorption coefficient by another order of magnitude, an effective slot half height of 4 mm is required, *i.e.*, the actual half height would have to be doubled, to roughly 5 mm.

4 Conclusions

In this article, we have expressed the desorption coefficient of a high-energy electron or positron storage ring in terms of the photoemission and the electron-induced gas-desorption yields of the vacuum-chamber material. Both these quantities can be measured in the laboratory prior to accelerator construction.

The expression derived was used to estimate the gas resorption in the main damping rings of the Next Linear Collider. An increase of the absorber-slot height by a factor of 2 was shown to reduce the resorption coefficient by an order of magnitude. Since chamber prototypes for the NLC damping rings are not yet available, for this example we had to rely on approximations to measured properties of aluminum that we found in the literature.

Acknowledgements

The author thanks Tor Raubenheimer for suggesting this study, for helpful discussions, and for urging him to publish the results. He is also grateful to Wolfgang Stoeffl for some valuable comments.

References

- [1] J. Kouptsidis and G.A. Mathewson, “Reduction of the photoelectron induced gas resorption in the PETRA vacuum system by in situ argon glow discharge cleaning”, DESY internal report, DESY 76/49, unpublished (1976).
- [2] O. Gröbner, “Vacuum Systems”, CERN accelerator school, Gif-sur-Yvette, CERN report 85-19, unpublished (1985).
- [3] PEP-II Conceptual Design Report, SLAC Internal Report SLAC-418, unpublished (1993).
- [4] See, for instance: D. Degèle, “DORIS, Present Status and Future Plans”, Proc. of the IXth International Conference on High Energy Accelerators, p. 43 (1974).
- [5] W.T. Weng et al., “Beam stability at SRRC storage ring”, presented at PAC 95, Dallas (1995).
- [6] D. Sagan and A. Temnykh, “Observations of the coherent beam-ion interaction in the CESR storage ring”, Nucl. Instr. and Methods A 344 p. 459 (1994).
- [7] T. Raubenheimer and F. Zimmerman, “Fast Beam-Ion Instability. I. Linear Theory and Simulations”, Phys. Rev. E 52, 5, p. 5487 (1995); G. Stupakov, T. Raubenheimer and F. Zimmerman, “Fast Beam-Ion Instability. II. Effect of Ion Decoherence” Phys. Rev. E 52, 5, p. 5499(1995);
- [8] O. Gröbner, A.G. Mathewson, P. Strubin, and E. Alge, R. Souchet, “Neutral gas resorption and photoelectric emission from aluminum al-

- loy vacuum chambers exposed to synchrotron radiation”, *J. Vac. Sci. Technol. A* 7 (2) p. 223 (1989).
- [9] T. Raubenheimer et al., “A damping ring design for the SLAC Next Linear Collider”, presented at PAC 95, Dallas, and SLC Internal Report SLAC-PUB-95-6848, unpublished (1995).
- [10] The ZDR Design Group, “Zeroth-Order Design Report for the Next Linear Collider”, Internal SLAC Report, unpublished (1996).
- [11] M.-H. Achard, R. Calder, and A. Mathewson, *Vacuum* 29 (2), 53 (1979).
- [12] W. Stoeffl, private communication (1996).
- [13] M. Sands, “The Physics of Electron Storage Rings”, SLAC-121 (1971).
- [14] G.A. Schott, “Electromagnetic Radiation”, Cambridge University Press (1912).
- [15] J. Schwinger, *Phys. Rev.* 75,1912 (1949).
- [16] J.D. Jackson, “Classical Electrodynamics”, 2nd ed., J. Wiley, N.Y. (1975).
- [17] W. Stoeffl, private communication (1996).
- [18] G.L. Weessler, “Photoionization in Gases and Photoelectric Emission from Solids”, in S. Flügge (ed.), “Handbuch der Physik”, Bd. 21 “Elektronen-Emission, Gasentladungen I”, p. 376 (1956).
- [19] C.L. Foerster, et al., *Journal of Vacuum and Science Technology A* 8 (3), 2856 (1990).
- [20] K. Ohmi, “Beam and photoelectron interactions in positron storage rings,” *Phys. Rev. Lett.* 75, p. 1526 (1995).

- [21] T. Raubenheimer et al., “Collective instabilities in the NLC damping ring designs,” presented at PAC95 Dallas, SLAC Internal Report SLAC-PUB-95-6843, unpublished (1995).
- [22] Landolt-Börnstein, “Zahlenwerte und Funktionen”, 6. Teil, “Elektrische Eigenschaften I“, K.H. Hellwege and A.M. Hellwege (ed.), p. 991 (1959).
- [23] J.A.R. Samson, “Atomic Photoionization”, in S. Flügge (ed.), “Handbuch der Physik”, Bd. 31 “Korpuskeln und Strahlung in Materie I“, p. 154 (1982).
- [24] M.-H. Achard, “Resorption des gaz induite par des electrons et des ions de l’acier inoxydable, du coivre OFHC, di titane et de l’ aluminium purs”, CERN Internal Report CERN-ISR-VA 76-34, unpublished (1976).
- [25] E. Garwin, E. Hoyt, M. Rabinowitz and J. Jurow, “Electron Induced Resorption of Gases from Aluminum”, SLAC Internal Report SLAC-PUB-392, unpublished (1968).
- [26] T. Raubenheimer, private communication (1995).

Parameter	Value
Energy E (GeV)	2
Circumference C (m)	220
Current I (A)	1.2
Horizontal equilibrium emittance $\gamma\epsilon_x$ (μm μrad)	3
Vertical equilibrium emittance $\gamma\epsilon_y$ (μm μrad)	0.02
Beam-pipe radius r (mm)	12.5
Cell length l (m)	3.9
Arc bending magnet angle α_B (mrad)	157
Arc bending radius ρ (m)	4.4
Design absorber-slot half height w (mm)	2.5
Design Average Arc Pressure (nTorr)	0.7

Table 1: Selected parameters of the NLC main damping rings.

Figure Captions

Figure 1. Layout of a standard cell in the NLC main damping ring showing magnet and vacuum chamber components; from Ref. [10].

Figure 2. Damping-ring vacuum chamber and antechamber in a quadrupole magnet; from Ref. [10].

Figure 3. Schematic of the synchrotron-radiation fan generated in a bending magnet, which may hit the vacuum chamber in the same bend (case 1), in the straight section behind (case 2) or in the next bend (case 3); the corresponding distances traversed by the photons before impacting on the vacuum chamber are denoted d_1, d_2 and d_3 . The minimum vertical emission angle for resorption is $\theta_{min} = w/d_i (i = 1, 2, 3)$, where w signifies the absorber-slot half height.

Figure 4. Minimum vertical photon emission angle to strike the vacuum chamber, Eq. (12), as a function of the position along the bend (in radian) for three different values of the absorber-slot half height w . In the present design, the half height w is nominally chosen as 2.5 mm. Chamber misalignments and closed-orbit distortions reduce it to an effective value of about 1.5 mm. The very short constant lines on the far left, *i.e.*, at $\alpha \leq 0.003$, apply for photons emitted at the very end of the bending magnet, which propagate to the next bend before they impinge on the beam pipe.

Figure 5. Number of photons striking the vacuum chamber per electron and radian, Eq. (8), as a function of the minimum emission angle θ_{min} .

Figure 6. Measured photoemission yield for aluminum [1, 22, 23] and approximate parametrization, Eq. (13), as a function of the photon energy.

Figure 7. Approximate number of photoelectrons per electron and radian, Eq. (9), as a function of minimum emission angle θ_{min} for an aluminum vacuum chamber.

Figure 8. Measured electron-induced gas desorption from pure aluminum after two different treatments as a function of electron energy E_e [24], and approximate parametrization, Eq. (14).

Figure 9. Number of desorbed molecules per electron and radian, Eq. (10), as a function of the minimum emission angle θ_{min} .

Figure 10. Estimated resorption coefficient, Eq. (11), for the NLC main damping rings as a function of the absorber-slot half height w . In the present design the half height is nominally chosen as 2.5 mm, which is reduced to an effective value of 1.5 mm by closed-orbit distortions and chamber misalignments.

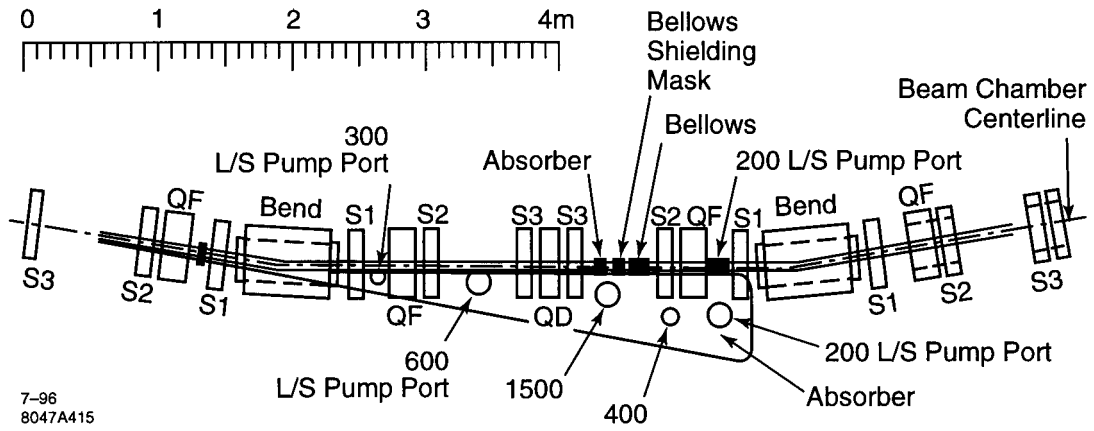


Figure 1

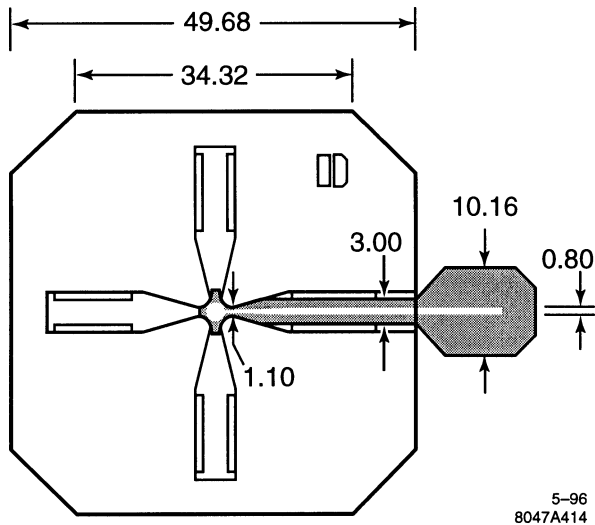


Figure 2

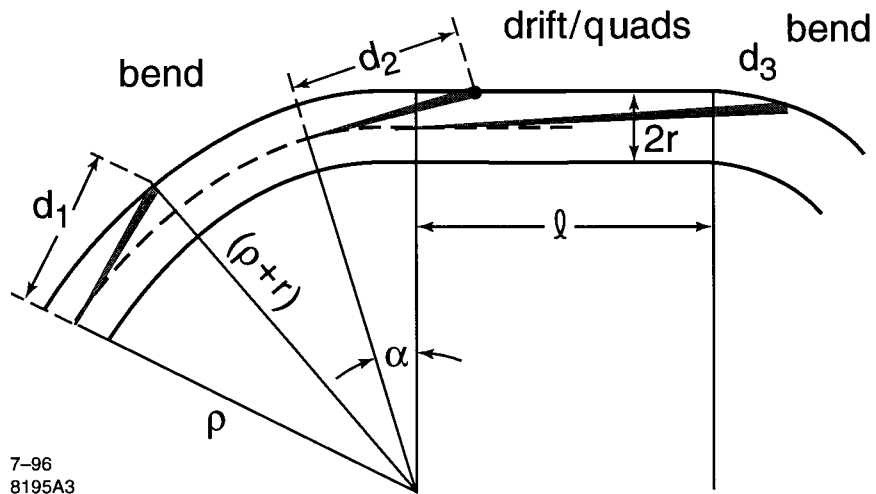


Figure 3

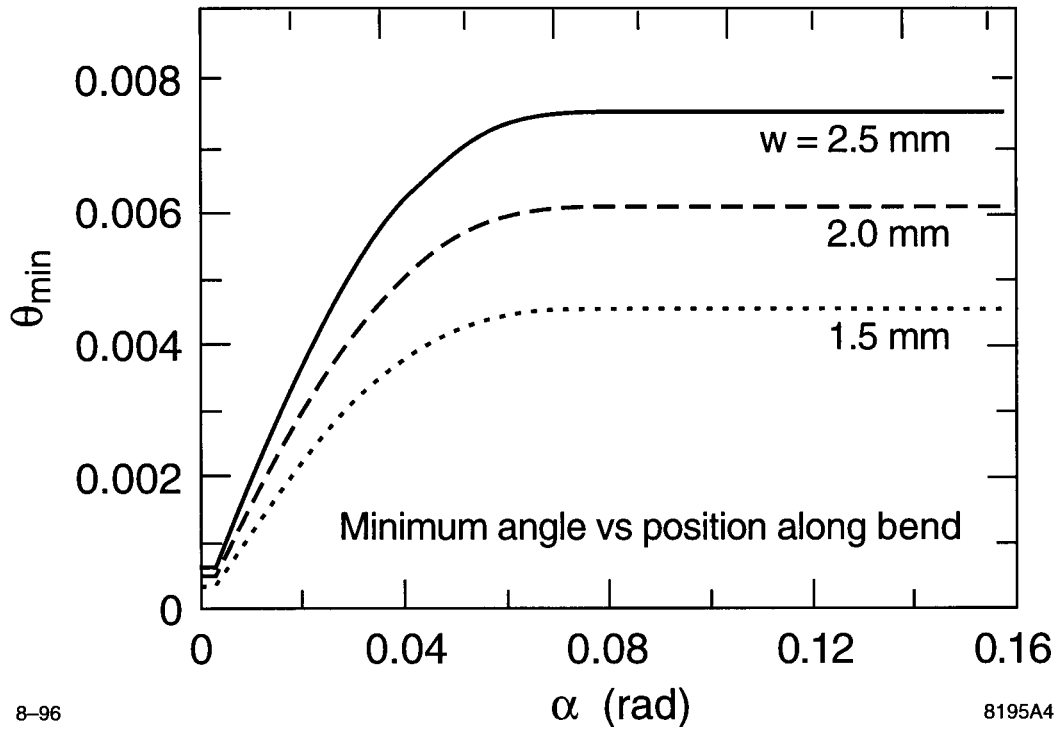
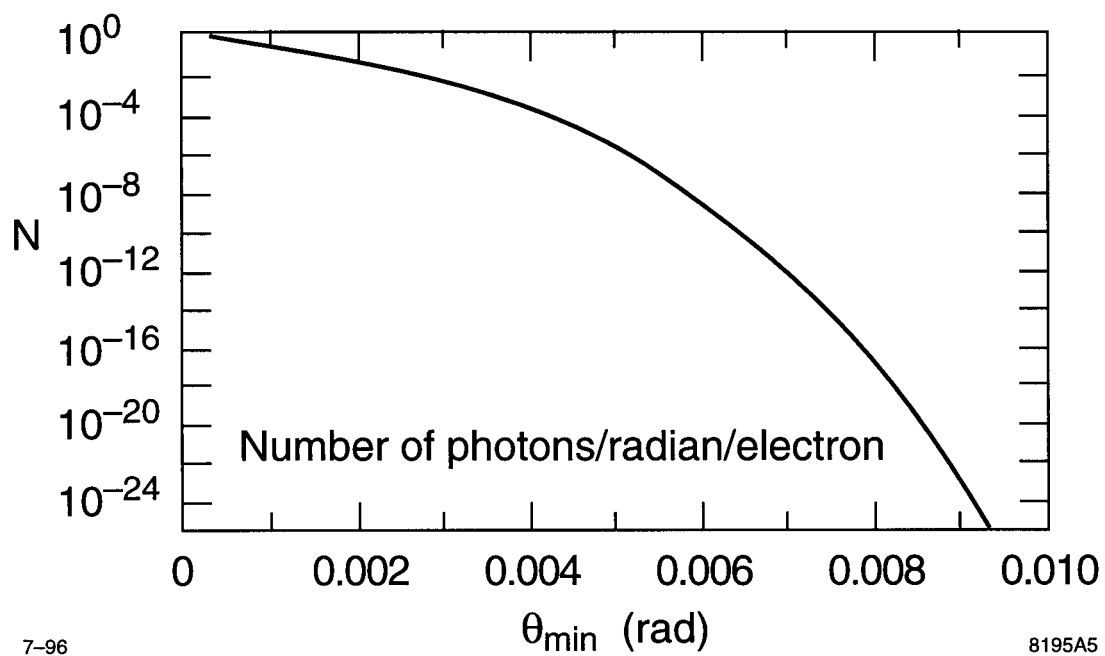


Figure 4



7-96

8195A5

Figure 5

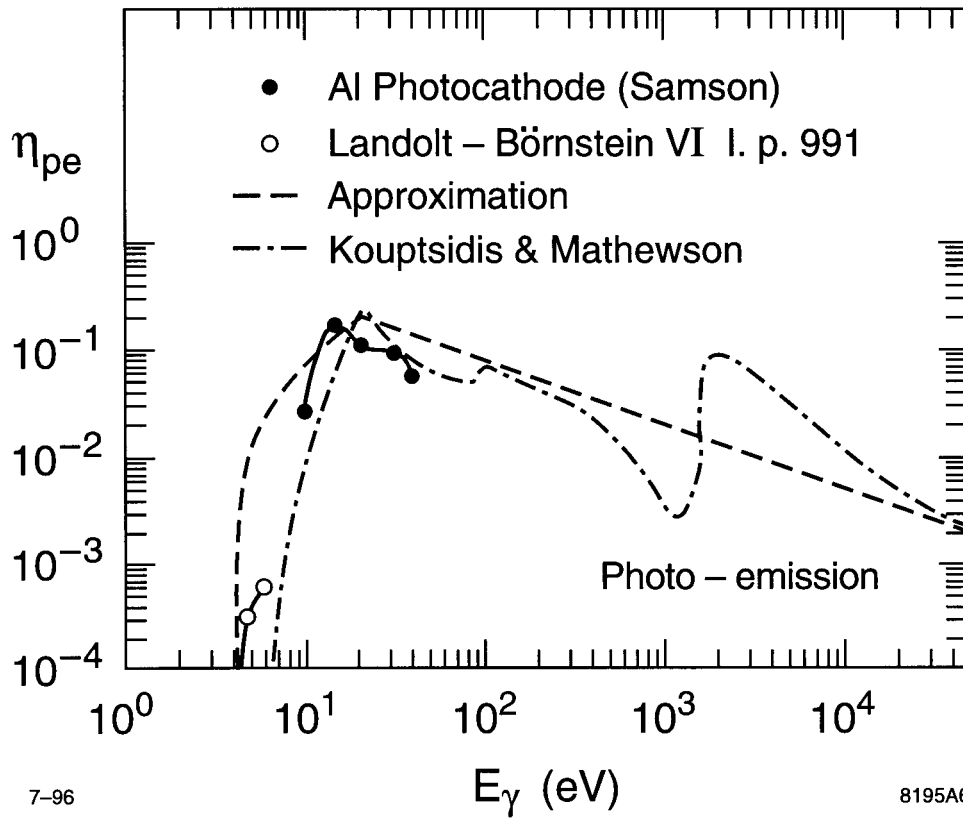


Figure 6

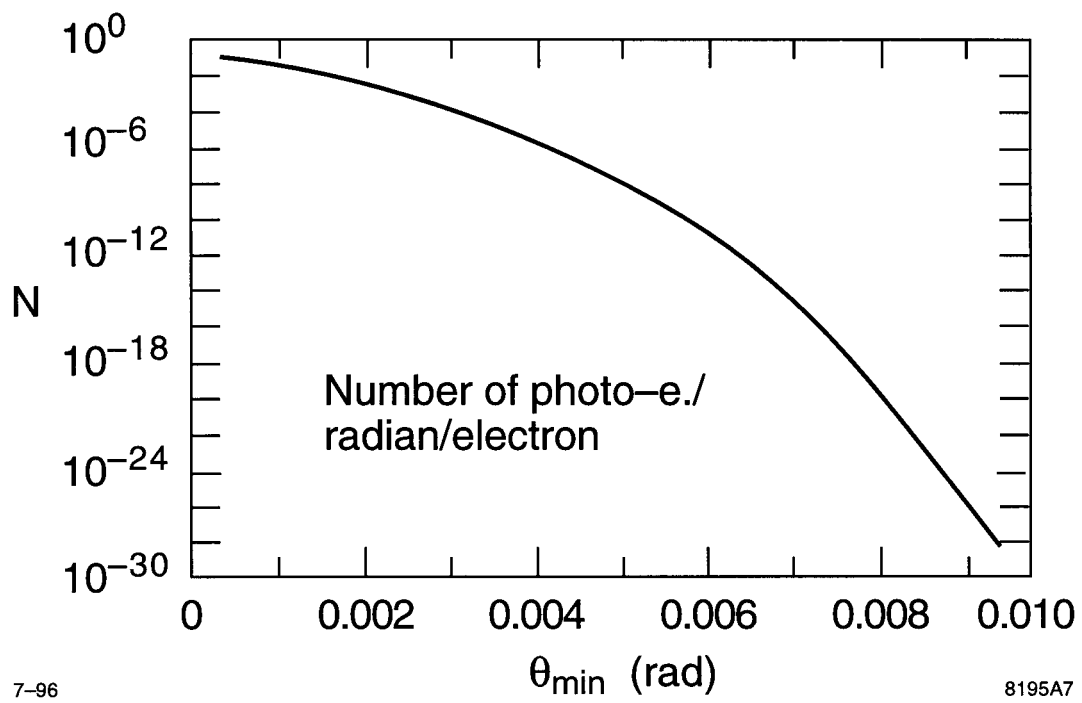


Figure 7

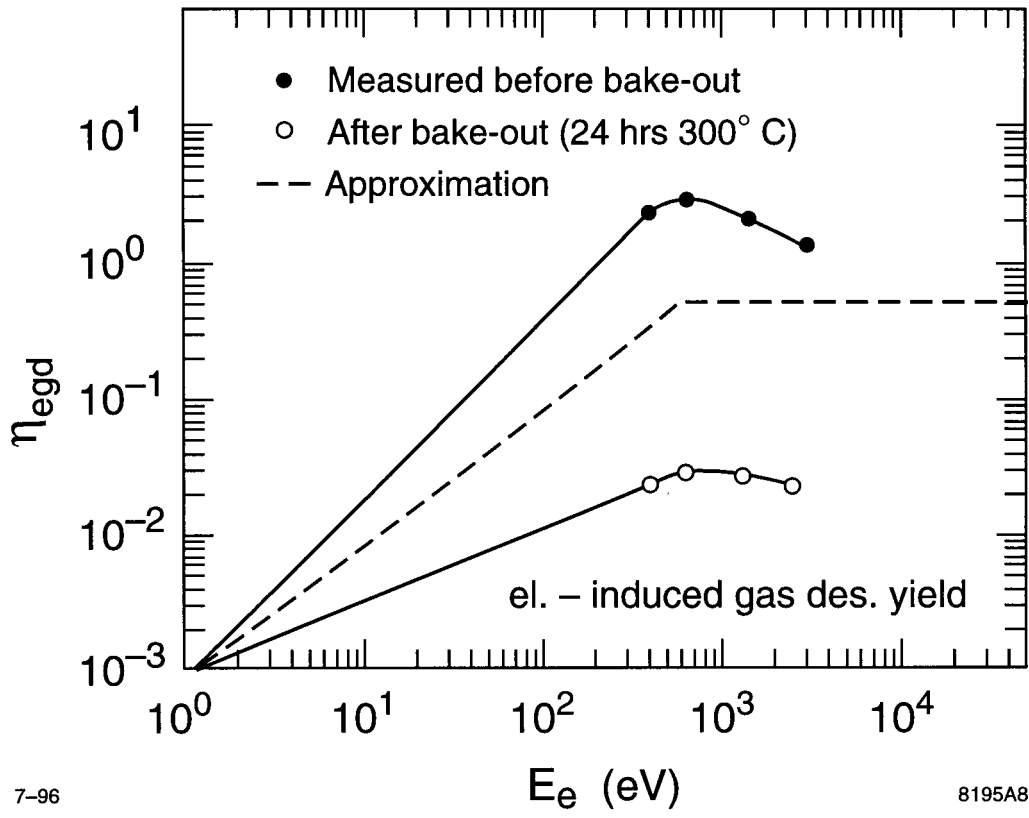


Figure 8

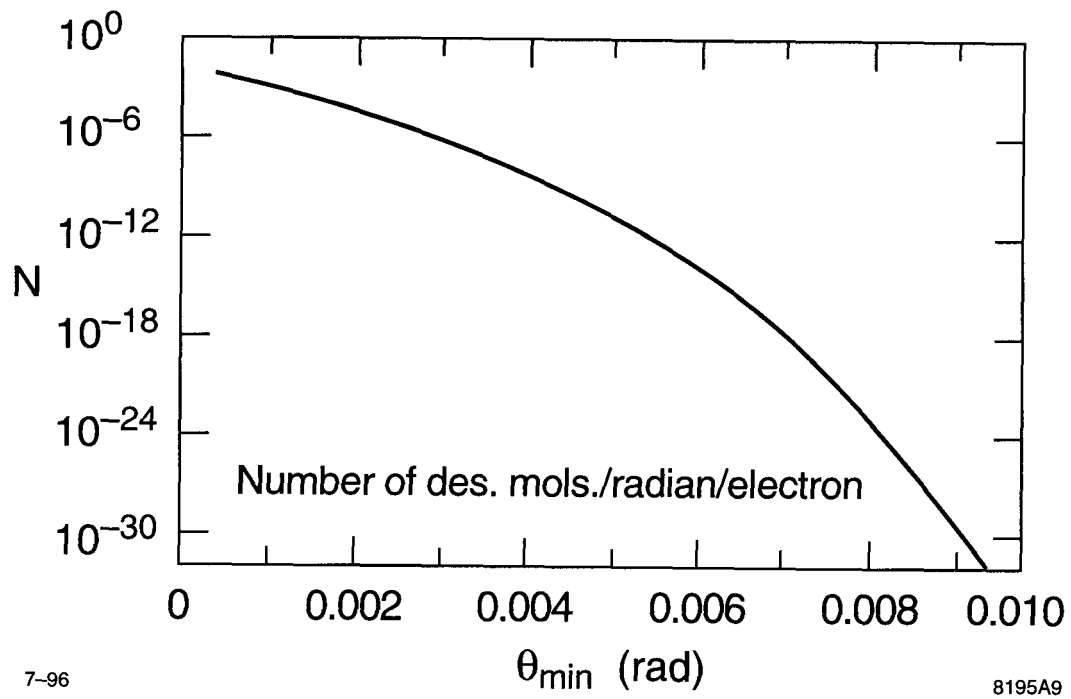


Figure 9

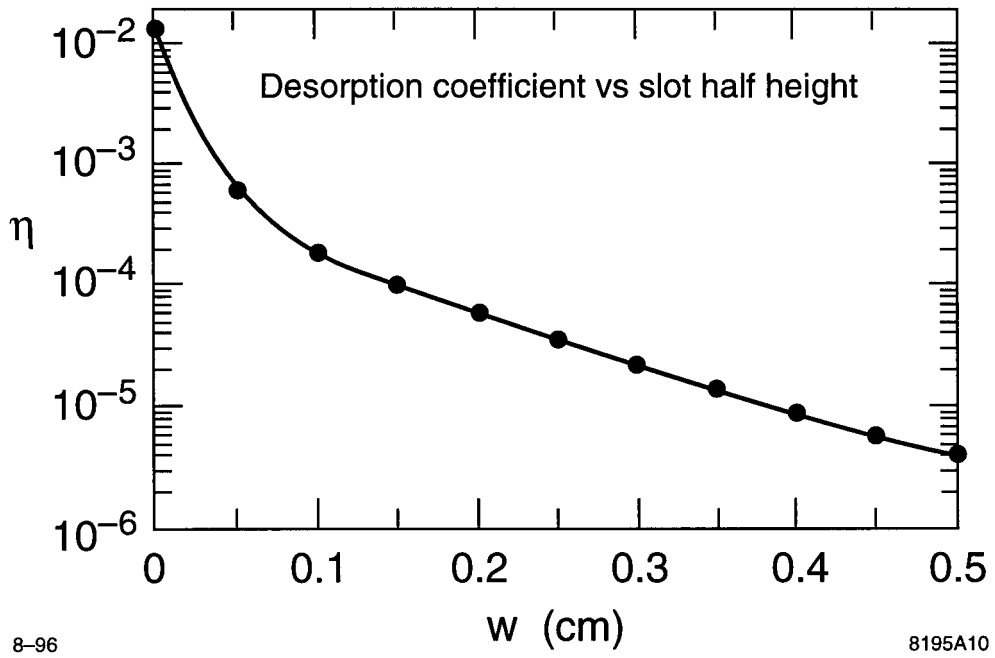


Figure 10